Signal Processing 157 (2019) 88–96

Contents lists available at ScienceDirect

Signal Processing

journal homepage: www.elsevier.com/locate/sigpro

Transmit beamspace-based DOD and DOA estimation method for bistatic MIMO radar

Baoqing Xu[a], Yongbo Zhao[a,b,*]

[a] National Lab of Radar Signal Processing, Xidian University, Xi'an 710071, People's Republic of China
[b] Collaborative Innovation Center of Information Sensing and Understanding, Xidian University, Xi'an 710071, People's Republic of China

ARTICLE INFO

Article history:
Received 21 April 2018
Revised 13 November 2018
Accepted 20 November 2018
Available online 22 November 2018

Keywords:
Multiple-input multiple-output radar
Angle estimation
Transmit beamspace design
DOD estimation error compensation

ABSTRACT

In this paper, we propose a novel angle estimation method in bistatic multiple-input multiple-output (MIMO) radar, which combines the transmit beamspace (TB) technique with the unitary ESPRIT (U-ESPRIT) model. The TB matrix is designed to focus the transmitted energy within the desired spatial sector, thus achieving the transmit coherent gain. Due to the special data structure of the TB-based bistatic MIMO radar, a corresponding method is proposed to construct the real-valued model. Unfortunately, the existed interpolation error inevitably degrades the direction-of-departure (DOD) estimation performance. To compensate the DOD estimation error, a look-up table is created, which establishes a one-to-one mapping relationship for DOD. The Cramer-Rao bound (CRB) on angle estimation in TB-based bistatic MIMO radar is also derived for performance analysis. Compared with existing methods, the proposed algorithm has better estimation performance due to the improved signal-to-noise ratio (SNR) gain and requires less computational complexity. Numerical simulations are presented to demonstrate the estimation performance of the proposed algorithm.

1. Introduction

Multiple-input multiple-output (MIMO) radar transmits multiple transmit waveforms and has attracted considerable attention in recent years [1–4]. According to the configuration of transmit and receive arrays, MIMO radar systems can be divided into two categories: statistical MIMO radar [5] and colocated MIMO radar [6]. Due to the widely spaced transmit and receive antennas, the spatial diversity gain is achieved in statistical MIMO radar. In contrast with statistical MIMO radar, the transmit and receive antennas in colocated MIMO radar are closely spaced. Colocated MIMO radar employs waveform diversity and the spatial resolution of radar is thus improved. This paper addresses the problem of direction-of-departure (DOD) and direction-of-arrival (DOA) estimation in bistatic MIMO radar, which is one kind of colocated MIMO radar.

The DOD and DOA estimation problem in bistatic MIMO radar has been investigated for many years and many methods have been proposed. In [7], a two-dimensional (2-D) search method is proposed for DOD and DOA estimation, which requires huge computational complexity. To solve this problem, a polynomial root finding algorithm is proposed in [8]. The problem of 2-D search is solved by finding the roots of the polynomial function. In [9], the ESPRIT algorithm is proposed for angle estimation in bistatic MIMO radar. This algorithm owns good estimation performance, but additional angle pairing is required. Based on [9], a modified ESPRIT algorithm is proposed in [10] and angle pairing can be automatically achieved. In [11], the unitary ESPRIT (U-ESPRIT) algorithm is proposed based on the real-valued signal model, which is obtained by unitary transformation. Exploiting the forward-backward averaging technique, the U-ESPRIT algorithm can also deal with a maximum of two coherent targets.

Exploiting the multidimensional structure of the received data, a series of tensor-based methods have been proposed in [12–15]. All these methods construct the tensor signal model and use tensor decomposition techniques [16], which mainly include higher-order singular value decomposition (HOSVD) and parallel factor (PARAFAC) decomposition. In [12], a multi-SVD method is proposed, which provides accurate estimation of the signal subspace compared with traditional subspace-based methods. Extending the forward-backward averaging technique to tensor case, the unitary tensor-ESPRIT (UTE) algorithm is presented in [13]. The constructed real-valued tensor signal model is decomposed through HOSVD, which can obtain the signal subspace with higher precision. In [14], the PARAFAC algorithm is proposed for angle estimation in bistatic MIMO radar. Without calculating the signal subspace, the PARAFAC algorithm owns excellent performance especially at low signal-to-noise ratio (SNR). Combining the forward-backward av-

* Corresponding author.
E-mail address: ybzhao@xidian.edu.cn (Y. Zhao).

https://doi.org/10.1016/j.sigpro.2018.11.016
0165-1684/

eraging technique with the PARAFAC model, the unitary PARAFAC (U-PARAFAC) algorithm is proposed in [15], which owns superior performance especially in dealing with highly correlated targets. All the methods in [7–15] are proposed with the assumption that the additive noise follows white Gaussian distribution. In [17], the angle estimation method is proposed in the presence of spatial colored noise. The ability of suppressing the colored noise is enhanced by utilizing the tensor structure.

Unfortunately, all the methods mentioned above are based on traditional bistatic MIMO radar, which exploits full waveform diversity and results in flat transmit gain in all directions. That is to say, the transmit waveforms in [7–15] are mutually orthogonal, which actually sacrifices the transmit coherent gain and degrades the estimation accuracy. In [18,19], the transmit beamspace (TB) technique is applied in monostatic MIMO radar and is not extended to bistatic MIMO radar. Moreover, both methods in [18,19] do not combine the real-valued U-ESPRIT model. In practice, the general spatial sector where the targets are located can often be determined. Under this condition, it will cause undesirable energy waste when still using the orthogonal transmit waveforms.

In this paper, the proposed algorithm is designed with white Gaussian noise. The signal model of the proposed TB-based bistatic MIMO radar is firstly constructed. Then, the TB matrix is designed to focus the transmitted energy within the desired spatial sector. Due to the special data structure of the TB-based bistatic MIMO radar, a corresponding method is proposed to construct the real-valued U-ESPRIT model. Because the interpolation error will degrade the DOD estimation accuracy, a DOD look-up table is created which establishes a one-to-one mapping relationship for DOD. Based on this table, when the DOD of the targets is estimated, more accurate DOD estimation can be achieved through mapping operation. We also derive the Cramer-Rao bound (CRB) on DOD and DOA estimation in TB-based bistatic MIMO radar. The performance analysis of the proposed algorithm in spatial colored noise is also given. Numerical simulations are presented to demonstrate the improved estimation accuracy of the proposed algorithm.

Notations: Scalars are denoted by italic letters, vectors by lowercase boldface letters and matrices by uppercase boldface letters. Notations $(\cdot)^T$, $(\cdot)^H$, $(\cdot)^*$ and $(\cdot)^{-1}$ denote transpose, Hermitian transpose, complex conjugate and matrix inversion, respectively. Symbols $\otimes$, $\odot$ and $\oplus$ represent Kronecker product, Khatri-Rao product and Hadamard product, respectively. $\mathrm{vec}(\cdot)$ and $\mathrm{diag}(\cdot)$ respectively denote the vectorization operation and the diagonalization operation. The real part and imaginary part of a complex vector or matrix are denoted by $\mathrm{Re}\{\cdot\}$ and $\mathrm{Im}\{\cdot\}$, respectively. $\mathrm{tr}(\cdot)$ denotes the trace of a matrix. $\mathbf{I}_n$ denotes the $n \times n$ identity matrix and $\|\cdot\|$ represents the Frobenius norm.

2. Signal model

The signal model of the proposed TB-based bistatic MIMO radar is built firstly in this section. Assume that a bistatic MIMO radar system is equipped with M transmit antennas and N receive antennas. The receive array is a half-wavelength spaced uniform linear array (ULA), while the configuration of the transmit array is not fixed for the proposed TB-based bistatic MIMO radar.

In TB-based bistatic MIMO radar, M transmit waveforms are not mutually orthogonal and can be expressed as $\sqrt{E/L}\mathbf{W}^*\mathbf{S}$, where $\mathbf{W} \in \mathbb{C}^{M\times L}$ denotes the TB matrix and L is called the number of transmit beams (or the transmit beamspace dimension). E denotes the total transmitted energy. Here, $\mathbf{S} = [\mathbf{s}_1(t), \mathbf{s}_2(t), \ldots, \mathbf{s}_L(t)]^T \in \mathbb{C}^{L\times T}$ denotes L orthogonal waveforms and has the property $\mathbf{S}\mathbf{S}^H = \mathbf{I}_L$. T denotes the number of samples per pulse period. Assume that there are K targets located in the far-field and the DOD and DOA of the kth target are denoted by θ_k and φ_k. The configuration of

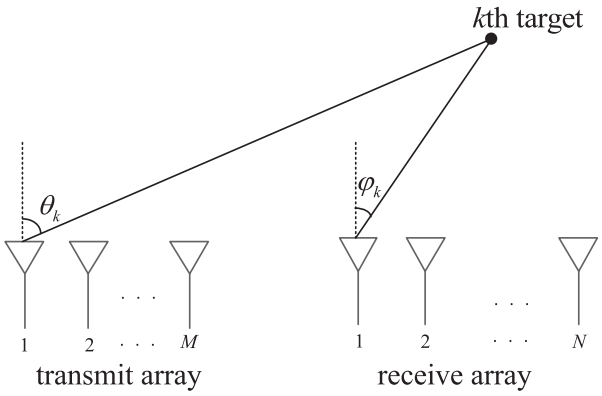

Fig. 1. The configuration of bistatic MIMO radar.

bistatic MIMO radar is shown in Fig. 1. The total number of pulses in a coherent processing interval (CPI) is Q. Then, the signal that reaches the kth target can be written as $\sqrt{E/L}\mathbf{a}^T(\theta_k)\mathbf{W}^*\mathbf{S}$. Assume that the K targets are located in the same range bin, the received signal can be modeled as

$$\mathbf{X}_q = \sqrt{E/L}\sum_{k=1}^{K}\alpha_{k,q}\mathbf{b}(\varphi_k)\mathbf{a}^T(\theta_k)\mathbf{W}^*\mathbf{S} + \mathbf{N}_q \tag{1}$$

where $\alpha_{k,q}$ denotes the reflection coefficient of the kth target in the qth pulse. Here, the reflection coefficients are assumed under the Swerling II target model, which remain unchanged in a CPI but vary independently from pulse to pulse. $\mathbf{a}(\theta_k)$ and $\mathbf{b}(\varphi_k)$ respectively denote the transmit and receive steering vectors of the kth target and $\mathbf{b}(\varphi_k)$ can be written as

$$\mathbf{b}(\varphi_k) = \left[e^{-j\pi\left(\frac{N-1}{2}\right)\sin\varphi_k}, \ldots, e^{-j\pi\sin\varphi_k}, 1, e^{j\pi\sin\varphi_k}, \ldots, e^{j\pi\left(\frac{N-1}{2}\right)\sin\varphi_k}\right]^T \tag{2}$$

Because the configuration of the transmit array is not fixed, the concrete form of $\mathbf{a}(\theta_k)$ is not given here. $\mathbf{N}_q$ represents the noise matrix in the qth pulse, which follows zero-mean white Gaussian distribution.

After that, (1) can be rewritten as

$$\mathbf{X}_q = \sqrt{E/L}\mathbf{B}\mathbf{\Lambda}_q\mathbf{A}^T\mathbf{W}^*\mathbf{S} + \mathbf{N}_q \tag{3}$$

where $\mathbf{A} = [\mathbf{a}(\theta_1), \mathbf{a}(\theta_2), \ldots, \mathbf{a}(\theta_K)]$ and $\mathbf{B} = [\mathbf{b}(\varphi_1), \mathbf{b}(\varphi_2), \ldots, \mathbf{b}(\varphi_K)]$ represent the transmit and receive steering matrices, respectively. In (3), $\mathbf{\Lambda}_q = \mathrm{diag}(\mathbf{c}_q)$, where $\mathbf{c}_q = [\alpha_{1,q}, \alpha_{2,q}, \ldots, \alpha_{K,q}]^T$.

Using the property $\mathbf{S}\mathbf{S}^H = \mathbf{I}_L$, (3) is right multiplied by $\mathbf{S}^H$ and then the output of matched filters can be written as

$$\begin{aligned}\mathbf{Y}_q &= \sqrt{E/L}\mathbf{B}\mathbf{\Lambda}_q\mathbf{A}^T\mathbf{W}^* + \overline{\mathbf{N}}_q \\ &= \sqrt{E/L}\mathbf{B}\mathbf{\Lambda}_q\left(\mathbf{W}^H\mathbf{A}\right)^T + \overline{\mathbf{N}}_q\end{aligned} \tag{4}$$

where $\overline{\mathbf{N}}_q = \mathbf{N}_q\mathbf{S}^H$ represents the noise term after matched filters. Vectorizing $\mathbf{Y}_q$, we have

$$\mathbf{y}_q = \sqrt{E/L}\left[\left(\mathbf{W}^H\mathbf{A}\right)\odot\mathbf{B}\right]\mathbf{c}_q + \overline{\mathbf{n}}_q \tag{5}$$

where $\mathbf{y}_q = \mathrm{vec}(\mathbf{Y}_q)$ and $\overline{\mathbf{n}}_q = \mathrm{vec}(\overline{\mathbf{N}}_q)$. Taking Q pulses into consideration, (5) can be rewritten compactly as

$$\mathbf{Y} = \sqrt{E/L}\left[\left(\mathbf{W}^H\mathbf{A}\right)\odot\mathbf{B}\right]\mathbf{C} + \tilde{\mathbf{N}} \tag{6}$$

where $\mathbf{Y}=[\mathbf{y}_1,\mathbf{y}_2,\ldots,\mathbf{y}_Q]$, $\mathbf{C}=[\mathbf{c}_1,\mathbf{c}_2,\ldots,\mathbf{c}_Q]$ and $\tilde{\mathbf{N}}=[\bar{\mathbf{n}}_1,\bar{\mathbf{n}}_2,\ldots,\bar{\mathbf{n}}_Q]$.

3. Proposed algorithm

In this section, a novel DOD and DOA estimation method is proposed for TB-based bistatic MIMO radar. Transmitted energy is focused within the desired spatial sector to improve the SNR gain. Due to the special data structure of the TB-based bistatic MIMO radar, the real-valued signal model is constructed with a corresponding method, which is different from traditional U-ESPRIT algorithm.

3.1. Transmit beamspace design

To focus the transmitted energy within the desired spatial sector, the TB matrix $\mathbf{W}$ is designed before DOD and DOA estimation. Firstly, we define a $L\times 1$ $(L<M)$ virtual steering vector

$$\bar{\mathbf{a}}(\theta)=\left[e^{-j\pi(\frac{L-1}{2})\sin\theta},\ldots,e^{-j\pi\sin\theta},1,e^{j\pi\sin\theta},\ldots,e^{j\pi(\frac{L-1}{2})\sin\theta}\right]^T \tag{7}$$

Similar with [20], we also define a unitary matrix $\mathbf{U}$ which can be written as

$$\mathbf{U}_{2n}=\frac{1}{\sqrt{2}}\begin{bmatrix}\mathbf{I}_n & j\mathbf{I}_n\\ \mathbf{\Pi}_n & -j\mathbf{\Pi}_n\end{bmatrix} \tag{8}$$

if the subscript is even, or

$$\mathbf{U}_{2n+1}=\frac{1}{\sqrt{2}}\begin{bmatrix}\mathbf{I}_n & \mathbf{0} & j\mathbf{I}_n\\ \mathbf{0}^{\mathrm{T}} & \sqrt{2} & \mathbf{0}^{\mathrm{T}}\\ \mathbf{\Pi}_n & \mathbf{0} & -j\mathbf{\Pi}_n\end{bmatrix} \tag{9}$$

if the subscript is odd. $\mathbf{\Pi}_n$ denotes the $n\times n$ exchange matrix having ones on its antidiagonal and zeros elsewhere. According to [20], $\mathbf{U}_L^H\bar{\mathbf{a}}(\theta)$ is a real-valued vector which is usually used for unitary transformation.

To guarantee the desired data structure, we try to minimize the difference between $\mathbf{W}^H\mathbf{a}(\theta)$ and $\mathbf{U}_L^H\bar{\mathbf{a}}(\theta)$ in the desired spatial sector. Additionally, we also need to constrain the level at which the transmitted energy is distributed outside the region of interest. For these two purposes, the TB matrix $\mathbf{W}$ is designed by solving the following convex optimization problem

$$\begin{aligned}&\min_{\mathbf{W}}\ \max_{j}\ ||\mathbf{W}^H\mathbf{a}(\theta_j)||,\ \theta_j\in\overline{\Theta},\ j=1,2,\ldots,J\\ &\text{s.t.}\quad ||\mathbf{W}^H\mathbf{a}(\theta_i)-\mathbf{U}_L^H\bar{\mathbf{a}}(\theta_i)||\le\beta,\ \theta_i\in\Theta,\ i=1,2,\ldots,I\end{aligned} \tag{10}$$

where Θ denotes the desired spatial sector and $\overline{\Theta}$ is the complement sector of Θ. I and J represent the numbers of grids of angles in Θ and $\overline{\Theta}$, respectively. The parameter β denotes the tolerable deviation between $\mathbf{W}^H\mathbf{a}(\theta)$ and $\mathbf{U}_L^H\bar{\mathbf{a}}(\theta)$ in Θ. The problem (10) can be efficiently solved by using interior-point methods [21]. It is important to emphasize that the constraint in (10) is to minimize the difference between $\mathbf{W}^H\mathbf{a}(\theta)$ and $\mathbf{U}_L^H\bar{\mathbf{a}}(\theta)$ instead of $\bar{\mathbf{a}}(\theta)$ in [18]. This directly results in the special data structure of the TB-based bistatic MIMO radar.

As mentioned above, the transmit waveforms in TB-based bistatic MIMO radar can be expressed as $\sqrt{E/L}\mathbf{W}^*\mathbf{S}$. Consequently, the total transmitted energy can be written as

$$(E/L)\mathrm{tr}(\mathbf{W}^*\mathbf{S}\mathbf{S}^H\mathbf{W}^T)=(E/L)\mathrm{tr}(\mathbf{W}\mathbf{W}^H) \tag{11}$$

To keep the total transmitted energy fixed at E, the obtained $\mathbf{W}$ after solving (10) should be scaled to satisfy $\mathrm{tr}(\mathbf{W}\mathbf{W}^H)=L$. It is noted that the TB matrix $\mathbf{W}$ can be calculated off-line and does not require real-time computation.

3.2. DOD and DOA estimation

After obtaining the TB matrix, we start to build the real-valued signal model. However, the data structure of $\mathbf{Y}$ is quite different from traditional bistatic MIMO radar and the conventional U-ESPRIT algorithm [11] cannot be directly used here. To solve this problem, we define

$$\overline{\mathbf{Y}}=[\mathbf{Y},(\mathbf{I}_L\otimes\mathbf{\Pi}_N)\mathbf{Y}^*\mathbf{\Pi}_Q] \tag{12}$$

From (12), we can find that the matrix $\overline{\mathbf{Y}}=[\overline{\mathbf{Y}}_1^T,\overline{\mathbf{Y}}_2^T,\ldots,\overline{\mathbf{Y}}_L^T]^T\in\mathbb{C}^{LN\times 2Q}$ is not centro-Hermitian [22] because $\mathbf{I}_L\otimes\mathbf{\Pi}_N\neq\mathbf{\Pi}_{LN}$. Therefore, the real-valued signal model cannot be constructed like [11] and should be built by a special way. The main reason is that the data structure of $\mathbf{Y}$ is quite different from traditional bistatic MIMO radar. Although $\overline{\mathbf{Y}}$ is not centro-Hermitian, each submatrix $\overline{\mathbf{Y}}_l\in\mathbb{C}^{N\times 2Q}$ in $\overline{\mathbf{Y}}=[\overline{\mathbf{Y}}_1^T,\overline{\mathbf{Y}}_2^T,\ldots,\overline{\mathbf{Y}}_L^T]^T$ is centro-Hermitian. Based on this fact, a new real-valued matrix can be defined as

$$\mathbf{Z}=\left(\mathbf{I}_L\otimes\mathbf{U}_N^H\right)\overline{\mathbf{Y}}\mathbf{U}_{2Q} \tag{13}$$

Up to now, the desired real-valued model is constructed and angle information can be extracted from this model. Neglecting the effect of interpolation error, we prove in Appendix A that (13) can be rewritten as

$$\mathbf{Z}=\sqrt{\frac{E}{L}}\left(\mathrm{Re}\left\{\mathbf{W}^H\mathbf{A}\right\}\odot\mathbf{U}_N^H\mathbf{B}\right)[\mathbf{C},\ \mathbf{C}^*\mathbf{\Pi}_Q]\mathbf{U}_{2Q}+\hat{\mathbf{N}} \tag{14}$$

where $\hat{\mathbf{N}}$ denotes the real-valued noise term defined in Appendix A. Based on (14), it can be found that matrices $\mathrm{Re}\{\mathbf{W}^H\mathbf{A}\}$ and $\mathbf{U}_N^H\mathbf{B}$ include DOD and DOA information, respectively. To estimate the DOD and DOA of the targets, we construct the covariance matrix of $\mathbf{Z}$, which can be expressed as $\mathbf{R}=(1/2Q)\mathbf{Z}\mathbf{Z}^H$. Then, the signal subspace $\mathbf{E}_s$ that contains angle information can be calculated by performing the eigenvalue decomposition (EVD) of $\mathbf{R}$. $\mathbf{E}_s$ is composed of the K eigenvectors of $\mathbf{R}$ corresponding to the K largest eigenvalues. From (14), we can find that $\mathrm{Re}\{\mathbf{W}^H\mathbf{A}\}\odot\mathbf{U}_N^H\mathbf{B}$ spans the same subspace with $\mathbf{E}_s$. Without considering the effect of interpolation error, there exists $\mathrm{Re}\{\mathbf{W}^H\mathbf{a}(\theta)\}=\mathbf{U}_L^H\bar{\mathbf{a}}(\theta)$. In this case, it has been proved in [20] that the following expressions hold

$$(\mathbf{K}_{t,1}\otimes\mathbf{I}_N)\mathbf{E}_s\mathbf{\Psi}_t=(\mathbf{K}_{t,2}\otimes\mathbf{I}_N)\mathbf{E}_s \tag{15}$$

$$(\mathbf{I}_L\otimes\mathbf{K}_{r,1})\mathbf{E}_s\mathbf{\Psi}_r=(\mathbf{I}_L\otimes\mathbf{K}_{r,2})\mathbf{E}_s \tag{16}$$

where matrices $\mathbf{K}_{t,1}$, $\mathbf{K}_{t,2}$, $\mathbf{K}_{r,1}$ and $\mathbf{K}_{r,2}$ are given by $\mathbf{K}_{t,1}=\mathrm{Re}\{\mathbf{U}_{L-1}^H\mathbf{J}_t\mathbf{U}_L\}$, $\mathbf{K}_{t,2}=\mathrm{Im}\{\mathbf{U}_{L-1}^H\mathbf{J}_t\mathbf{U}_L\}$, $\mathbf{K}_{r,1}=\mathrm{Re}\{\mathbf{U}_{N-1}^H\mathbf{J}_r\mathbf{U}_N\}$ and $\mathbf{K}_{r,2}=\mathrm{Im}\{\mathbf{U}_{N-1}^H\mathbf{J}_r\mathbf{U}_N\}$. Here, $\mathbf{J}_t=[\mathbf{0},\mathbf{I}_{L-1}]$ and $\mathbf{J}_r=[\mathbf{0},\mathbf{I}_{N-1}]$ are selection matrices. In (15) and (16), $\mathbf{\Psi}_t=\mathbf{T}^{-1}\mathbf{\Delta}_t\mathbf{T}$ and $\mathbf{\Psi}_r=\mathbf{T}^{-1}\mathbf{\Delta}_r\mathbf{T}$, where $\mathbf{T}$ is a $K\times K$ nonsingular matrix. The expressions of $\mathbf{\Delta}_t$ and $\mathbf{\Delta}_r$ are respectively given by

$$\mathbf{\Delta}_t=\mathrm{diag}\{\tan(\pi\sin\theta_1/2),\tan(\pi\sin\theta_2/2),\ldots,\tan(\pi\sin\theta_K/2)\} \tag{17}$$

$$\begin{aligned}\mathbf{\Delta}_r=\mathrm{diag}\{&\tan(\pi\sin\varphi_1/2),\tan(\pi\sin\varphi_2/2),\ldots,\\ &\tan(\pi\sin\varphi_K/2)\}\end{aligned} \tag{18}$$

Matrices $\mathbf{\Psi}_t$ and $\mathbf{\Psi}_r$ in (15) and (16) can be calculated easily by using the least squares (LS) method. When $\mathbf{\Psi}_t$ and $\mathbf{\Psi}_r$ are obtained, the simultaneous Schur decomposition (SSD) method [23] is used to estimate the joint eigenvalues of $\mathbf{\Psi}_t$ and $\mathbf{\Psi}_r$. After that, the estimated DOD and DOA of the targets can be paired successfully. Assume that the kth eigenvalue of $\mathbf{\Psi}_t$ and $\mathbf{\Psi}_r$ is denoted by η_k and

Table 1
The procedure of building the DOD look-up table.

Step 1: Sample the desired spatial sector Θ. The sampled true DOD is denoted by θ_i, $i = 1, 2, \ldots, I$. I represents the total number of samples and should be large enough to guarantee the DOD estimation accuracy.
Step 2: Insert θ_i to (22) and calculate γ_i by using the LS method.
Step 3: Calculate the corresponding mapped DOD $\overline{\theta}_i$ according to (23). Then, the mapping relationship between θ_i and $\overline{\theta}_i$ is obtained.
Step 4: Repeat Steps 2 and 3 until i reaches I.
Step 5: Form the DOD look-up table constructed by the true DOD θ and mapped DOD $\overline{\theta}$, which includes the mapping relationship between θ and $\overline{\theta}$.

μ_k, respectively. Then, the estimated DOD and DOA of the kth target are given by

$$\hat{\theta}_k = \arcsin\left[2\arctan(\eta_k)/\pi\right] \tag{19}$$

$$\hat{\varphi}_k = \arcsin\left[2\arctan(\mu_k)/\pi\right] \tag{20}$$

3.3. DOD estimation error compensation

In the subsection above, the DOD and DOA are estimated based on (15) and (16) with the assumption that $\mathbf{W}^H\mathbf{a}(\theta) = \mathbf{U}_L^H\bar{\mathbf{a}}(\theta)$. Unfortunately, $\mathbf{W}^H\mathbf{a}(\theta)$ is not exactly equal to $\mathbf{U}_L^H\bar{\mathbf{a}}(\theta)$ because of the inevitable interpolation error in solving (10). This will inevitably degrade the estimation performance.

It is observed from (14) that the interpolation error only affects the DOD estimation accuracy, so it is unnecessary to adopt a 2-D model like (13). To compensate the DOD estimation error, we can build a DOD look-up table by using a noiseless real-valued model, which establishes a one-to-one mapping relationship for DOD. This model only contains the DOD information and has the same data structure as the proposed TB-based bistatic MIMO radar. From (12) and (13), the mapping relationship can be determined by using the following real-valued and noiseless model

$$\mathbf{Y}_{map} = \left[\mathbf{W}^H\mathbf{a}(\theta_i)\mathbf{c},\ \left(\mathbf{W}^H\mathbf{a}(\theta_i)\mathbf{c}\right)^*\mathbf{\Pi}_Q\right]\mathbf{U}_{2Q} \tag{21}$$

where θ_i, $i = 1, 2, \ldots, I$, denotes the true DOD sampled in Θ and $\mathbf{c}$ is a $1 \times Q$ vector. It is noted that the sampling interval should meet the requirement for DOD estimation precision. To estimate the mapped DOD corresponding to θ_i, we construct the covariance matrix of $\mathbf{Y}_{map}$, which can be expressed as $\mathbf{R}_{map} = (1/2Q)\mathbf{Y}_{map}\mathbf{Y}_{map}^H$. Then, we calculate the dominated eigenvector corresponding to the largest eigenvalue of $\mathbf{R}_{map}$. In Appendix B, we prove that the dominated eigenvector of $\mathbf{R}_{map}$ spans the same subspace with $\mathrm{Re}\{\mathbf{W}^H\mathbf{a}(\theta_i)\}$ in the desired spatial sector. Consequently, instead of using (21), we can directly establish the mapping relationship using the following equation:

$$\gamma_i\mathbf{K}_{t,1}\mathrm{Re}\left\{\mathbf{W}^H\mathbf{a}(\theta_i)\right\} = \mathbf{K}_{t,2}\mathrm{Re}\left\{\mathbf{W}^H\mathbf{a}(\theta_i)\right\} \tag{22}$$

Finally, the corresponding mapped DOD can be written as

$$\overline{\theta}_i = \arcsin\left[2\arctan(\gamma_i)/\pi\right] \tag{23}$$

where $\overline{\theta}_i$ denotes the mapped DOD corresponding to the true DOD θ_i. For each θ_i sampled in Θ, the mapped DOD can be calculated according to (22) and (23). We have summarized the details on how to build the DOD look-up table in Table 1. Up to now, the look-up table can be built which including the mapping relationship between $\overline{\theta}_i$ and θ_i. Using this table, the influence of interpolation error between $\mathbf{W}^H\mathbf{a}(\theta)$ and $\mathbf{U}_L^H\bar{\mathbf{a}}(\theta)$ in Θ can be reduced greatly. Once the DOD of the targets are estimated from the noisy model according to (19), more accurate DOD estimation can be achieved through the mapping operation.

3.4. CRB and complexity analysis

In traditional bistatic MIMO radar, M orthogonal waveforms are emitted from transmit array. As a matter of fact, the signal model of traditional bistatic MIMO radar is a special case of (6) with $L = M$ and $\mathbf{W} = \mathbf{I}_M$. Compared with the signal model built in [24], there is only an extra normalization factor $\sqrt{E/L}$ needed to be considered. Then, the CRB on DOD and DOA estimation for traditional bistatic MIMO radar can be written as

$$\mathrm{CRB}_{Tra} = \frac{\sigma_n^2 M}{2QE}\left\{\mathrm{Re}\left\{(\mathbf{D}^H\mathbf{P}_\Omega^\perp\mathbf{D}) \oplus \mathbf{H}^T\right\}\right\}^{-1} \tag{24}$$

where $\mathbf{P}_\Omega^\perp = \mathbf{I}_{MN} - \mathbf{\Omega}(\mathbf{\Omega}^H\mathbf{\Omega})^{-1}\mathbf{\Omega}^H$ denotes the orthogonal projection matrix and $\mathbf{D} = [\mathbf{D}_t,\ \mathbf{D}_r]$. Here, $\mathbf{\Omega} = \mathbf{A} \odot \mathbf{B}$, $\mathbf{D}_t = \mathbf{A}' \odot \mathbf{B}$ and $\mathbf{D}_r = \mathbf{A} \odot \mathbf{B}'$, where $\mathbf{A}' = [\frac{d\mathbf{a}(\theta_1)}{d\theta_1}, \frac{d\mathbf{a}(\theta_2)}{d\theta_2}, \ldots, \frac{d\mathbf{a}(\theta_K)}{d\theta_K}]$ and $\mathbf{B}' = [\frac{d\mathbf{b}(\varphi_1)}{d\varphi_1}, \frac{d\mathbf{b}(\varphi_2)}{d\varphi_2}, \ldots, \frac{d\mathbf{b}(\varphi_K)}{d\varphi_K}]$, respectively. In (24), σ_n^2 denotes the noise variance and $\mathbf{H} = \begin{bmatrix}\mathbf{F} & \mathbf{F}\\ \mathbf{F} & \mathbf{F}\end{bmatrix}$, where $\mathbf{F} = \mathbf{C}\mathbf{C}^H/Q$. Importantly, we can find that (24) has the same form as the CRB derived in [24] if $E = M$.

To further analyze the performance of the proposed algorithm, we derive the CRB on angle estimation for TB-based bistatic MIMO radar. In (6), we have constructed the signal model for the proposed TB-based bistatic MIMO radar. Then, according to [25], the CRB on DOD and DOA estimation in TB-based bistatic MIMO radar can be derived as

$$\mathrm{CRB}_{TB} = \frac{\sigma_n^2 L}{2QE}\left\{\mathrm{Re}\left\{(\mathbf{G}^H\mathbf{P}_\mathbf{V}^\perp\mathbf{G}) \oplus \mathbf{H}^T\right\}\right\}^{-1} \tag{25}$$

where $\mathbf{P}_\mathbf{V}^\perp = \mathbf{I}_{LN} - \mathbf{V}(\mathbf{V}^H\mathbf{V})^{-1}\mathbf{V}^H$, and $\mathbf{G} = [\mathbf{G}_t,\ \mathbf{G}_r]$. Here, $\mathbf{V} = (\mathbf{W}^H\mathbf{A}) \odot \mathbf{B}$, $\mathbf{G}_t = (\mathbf{W}^H\mathbf{A}') \odot \mathbf{B}$ and $\mathbf{G}_r = (\mathbf{W}^H\mathbf{A}) \odot \mathbf{B}'$. Here, we emphasize that (24) and (25) hold true only for white Gaussian noise.

Finally, the computational complexity of the proposed algorithm is analyzed. Because the TB matrix $\mathbf{W}$ and look-up table can be designed offline, the computational complexity of the proposed algorithm is mainly dominated by the construction and EVD of the covariance matrix $\mathbf{R}$. The total computational complexity of the proposed algorithm is $O(L^3N^3 + 2QL^2N^2)$, which is smaller than $O(M^3N^3 + 2QM^2N^2)$ of the traditional U-ESPRIT algorithm. Since the number of transmit beams L is usually smaller than the number of transmit antennas M, the proposed algorithm requires less computational complexity than the traditional U-ESPRIT algorithm. The computational complexity of the U-PARAFAC algorithm is $O(6MNQK + 27K^6)$ for each iteration, which causes huge computational cost when the number of iterations is considered.

4. Simulation results

In this section, numerical examples are presented to assess the estimation performance of the proposed algorithm. To compare the estimation performance of the proposed algorithm, the U-ESPRIT algorithm [11], the UTE algorithm [13], and the U-PARAFAC algorithm [15] are carried out. Moreover, the CRB of traditional bistatic MIMO radar (24) and the CRB of the proposed TB-based bistatic MIMO radar (25) are also used for performance analysis. To ensure the comparability of all the tested methods, both transmit and receive arrays in bistatic MIMO radar are half-wavelength spaced ULAs. Unless noted otherwise, the additive noise follows white Gaussian distribution with zero mean. We use the root mean square error (RMSE) to assess the performance of the tested methods. The RMSE of DOD is defined as

$$\mathrm{RMSE} = \sqrt{\frac{1}{PK}\sum_{k=1}^{K}\sum_{p=1}^{P}\left(\hat{\theta}_{k,p} - \theta_k\right)^2} \tag{26}$$

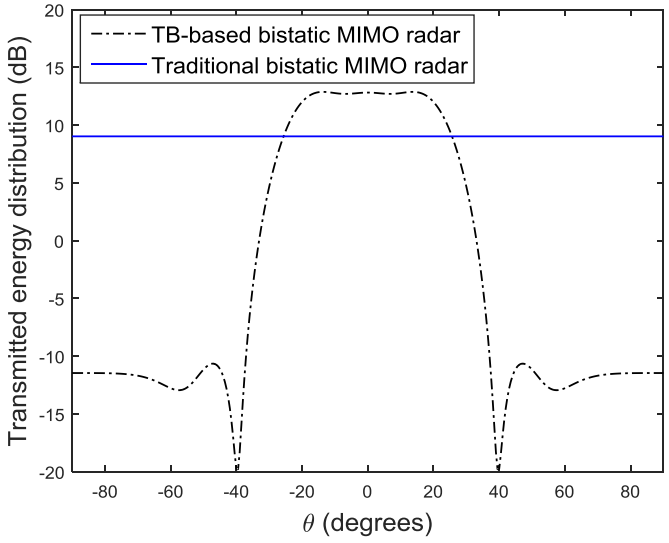

Fig. 2. Transmitted energy distribution for the traditional and TB-based bistatic MIMO radar with $\Theta = [-15^\circ,\ 15^\circ]$.

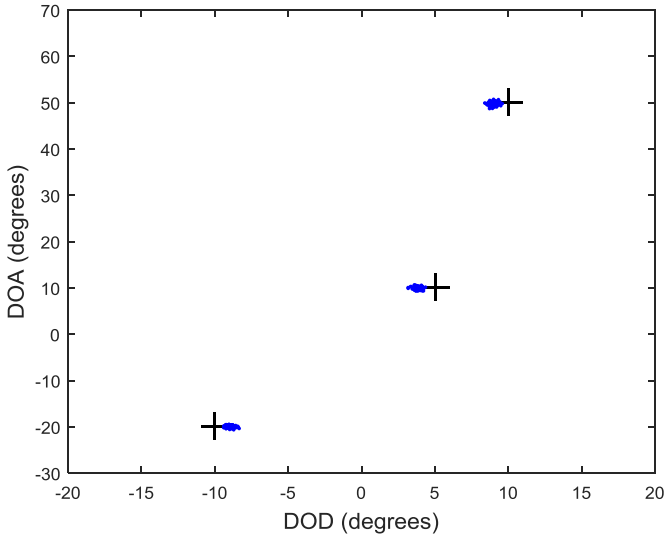

Fig. 3. Estimation results of the proposed algorithm before the mapping operation.

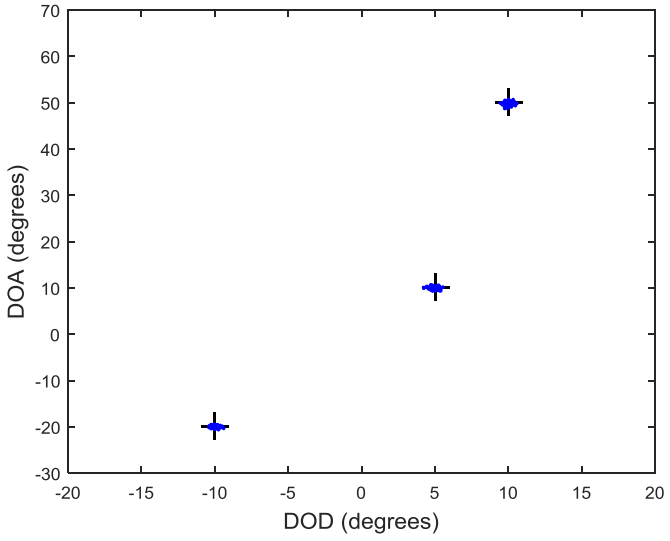

Fig. 4. Estimation results of the proposed algorithm after the mapping operation.

The RMSE expression for DOA is the same as (26) where the θ is replaced with φ. The RMSE of DOD and DOA is defined as

$$\text{RMSE} = \sqrt{\frac{1}{2PK}\sum_{k=1}^{K}\sum_{p=1}^{P}\left[\left(\hat{\theta}_{k,p}-\theta_k\right)^2+\left(\hat{\varphi}_{k,p}-\varphi_k\right)^2\right]} \tag{27}$$

where $\hat{\theta}_{k,p}$ and $\hat{\varphi}_{k,p}$ denote the estimated DOD and DOA in the pth Monte Carlo trial. The number of Monte Carlo trials is $P = 200$. In traditional bistatic MIMO radar, M orthogonal waveforms can be written as

$$\mathbf{s}_m(t) = \sqrt{\frac{1}{T}}e^{j2\pi\frac{m}{T}t},\ m = 1,\ 2,\ \ldots,\ M \tag{28}$$

In the proposed TB-based bistatic MIMO radar, only the first L orthogonal waveforms in (28) are used and the transmit waveforms can be formed as $\sqrt{E/L}\mathbf{W}^*\mathbf{S}$. For both traditional and TB-based bistatic MIMO radar, the total transmitted energy is fixed at $E = M$ in all examples, which means $\text{tr}(\mathbf{W}\mathbf{W}^H) = L$ according to (11). Then the transmitted energy distributed in θ for TB-based bistatic MIMO radar can be expressed as

$$P(\theta) = (E/L)||\mathbf{W}^H\mathbf{a}(\theta)||^2 \tag{29}$$

In all examples, the DOD of the targets is assumed to lie within a given spatial sector.

In all the examples, the TB matrix $\mathbf{W}$ is designed to focus the transmitted energy within $\Theta = [-15^\circ,\ 15^\circ]$. The number of transmit and receive antennas in bistatic MIMO radar is $M = 8$ and $N = 4$, respectively. The transmit beamspace dimension is chosen as $L = 6$ and the positive parameter is set as $\beta = 0.06$. When the TB matrix $\mathbf{W}$ is obtained by solving (10), the transmitted energy distribution for TB-based bistatic MIMO radar can be calculated according to (29). Fig. 2 shows the transmitted energy distribution for the traditional and TB-based bistatic MIMO radar. As shown in Fig. 2, the transmitted energy is successfully focused within the desired spatial sector in the TB-based bistatic MIMO radar, which can improve the SNR gain for the targets located in Θ.

In the first example, the necessity of mapping operation is evaluated. Assume that there are three uncorrelated targets located at $(\theta_1,\ \varphi_1) = (-10^\circ,\ -20^\circ)$, $(\theta_2,\ \varphi_2) = (5^\circ,\ 10^\circ)$ and $(\theta_3,\ \varphi_3) = (10^\circ,\ 50^\circ)$, respectively. The SNR of all three targets is fixed at 0 dB and the number of pulses is 50. Fig. 3 shows the estimation results of the proposed algorithm before taking the mapping operation. The number of Monte Carlo trials is 200. We observe from Fig. 3 that DOD estimation accuracy of the proposed algorithm is seriously degraded by the interpolation error, while the DOA estimation accuracy is not influenced. Then, we use the look-up table to map the estimation results shown in Fig. 3. Fig. 4 shows the estimation results of the proposed algorithm after the mapping operation. As demonstrated in Fig. 4, the DOD and DOA of the targets are estimated correctly. The DOD estimation error is compensated successfully based on the established mapping relationship. Comparing Fig. 4 with Fig. 3, it can be found that the DOD estimation error can be reduced greatly by using the look-up table.

In the second example, the estimation performance for uncorrelated targets is evaluated. Two uncorrelated targets are located at $(\theta_1,\ \varphi_1) = (-8^\circ,\ -30^\circ)$ and $(\theta_2,\ \varphi_2) = (12^\circ,\ 30^\circ)$, respectively. Fig. 5 shows the RMSE of DOD versus SNR before the mapping operation. Fig. 6 shows the RMSE of DOD versus SNR after the mapping operation. The number of pulses is fixed at 50. The CRB of traditional bistatic MIMO radar and the CRB of TB-based bistatic MIMO radar are also plotted for comparison. Fig. 7 shows the RMSE of DOA versus SNR with the number of pulses fixed at 50. As can be seen from Fig. 5, the DOD estimation performance of the proposed algorithm is degraded greatly especially in high

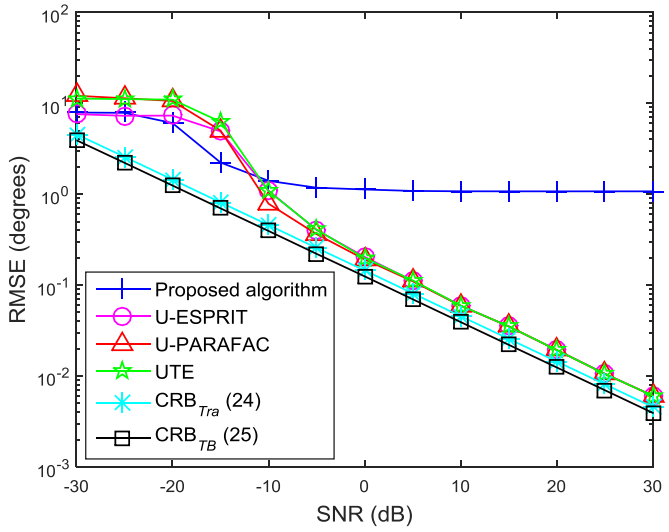

Fig. 5. RMSE of DOD versus SNR for two uncorrelated targets (before the mapping operation).

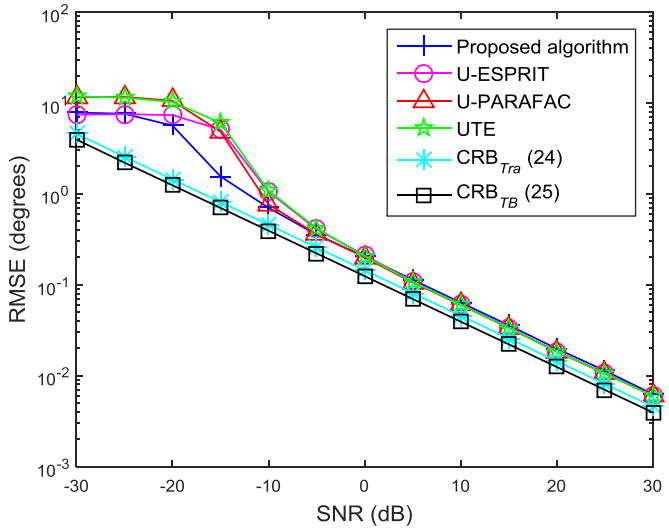

Fig. 6. RMSE of DOD versus SNR for two uncorrelated targets (after the mapping operation).

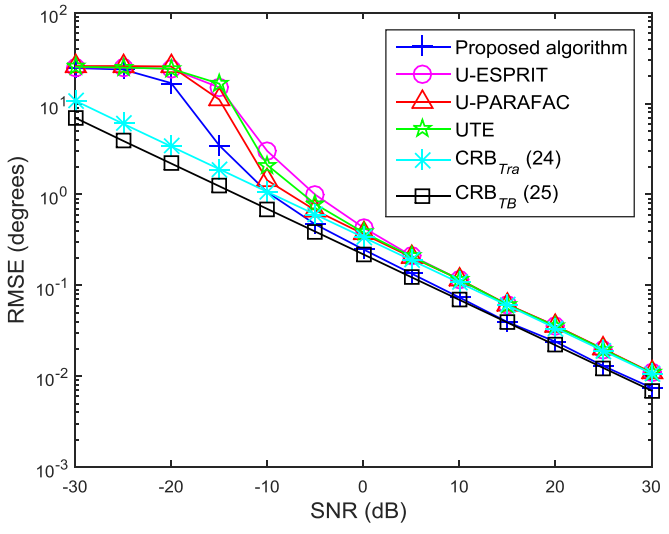

Fig. 7. RMSE of DOA versus SNR for two uncorrelated targets.

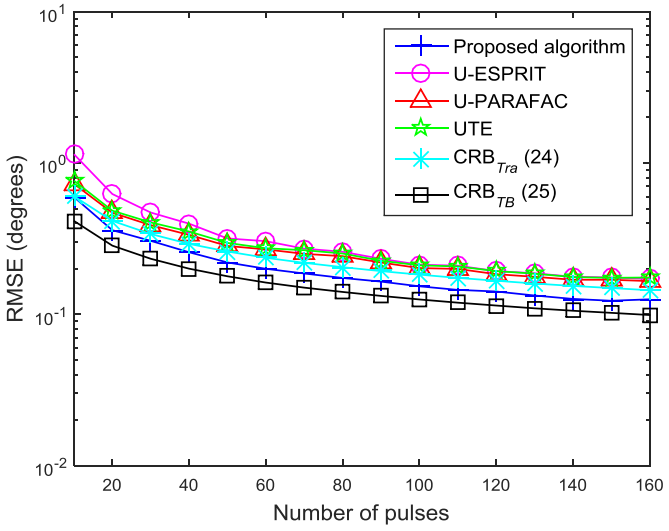

Fig. 8. RMSE versus the number of pulses for two uncorrelated targets.

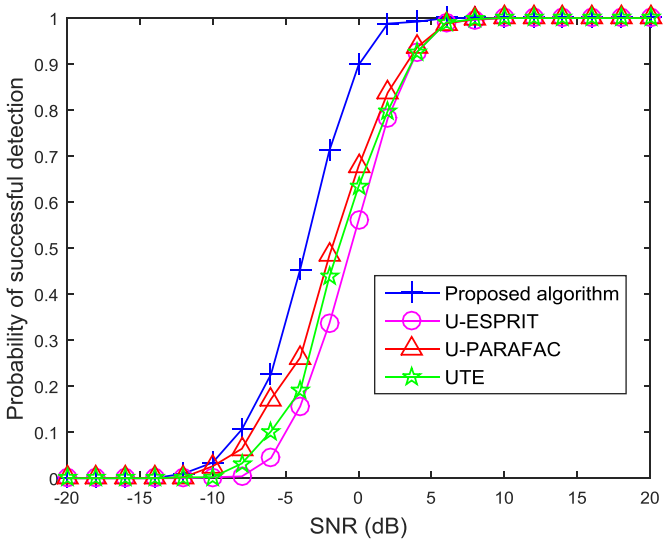

Fig. 9. Probability of successful detection versus SNR for two uncorrelated targets.

SNR region. This is consistent with the conclusions in [26]. At low SNR, the DOD estimation bias is dominated by noise effects. When SNR is larger than −20 dB, the estimation bias is dominated by the interpolation error. Comparing Fig. 5 with Fig. 6, we can find that the DOD estimation bias caused by interpolation error can be successfully compensated. The CRB of TB-based bistatic MIMO radar is lower than the CRB of traditional bistatic MIMO radar. This means that more accurate estimation can be achieved in the TB-based bistatic MIMO radar. Although the U-ESPRIT algorithm, the U-PARAFAC algorithm and the UTE algorithm are all based on the real-valued signal model, the TB technique is not applied in these methods. The proposed algorithm has better estimation performance than other methods due to the transmit coherent gain, which cannot be obtained in traditional bistatic MIMO radar.

Fig. 8 shows the RMSE of DOD and DOA versus the number of pulses. The SNR is fixed at 0 dB, while the number of pulses is varied from 10 to 160. Fig. 9 demonstrates the probability of successful detection versus SNR. If the absolute errors of DOD and DOA for both two targets are within 0.5°, it indicates that both two targets can be successfully detected. As shown in Fig. 9, all the methods have 100% successful detection in high SNR region. The probability of successful detection starts dropping at a certain point, which is

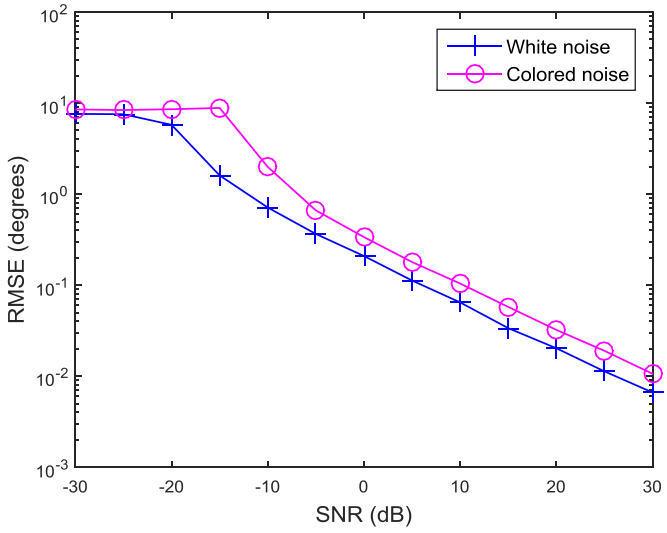

Fig. 10. DOD estimation performance of the proposed algorithm for white and colored noise.

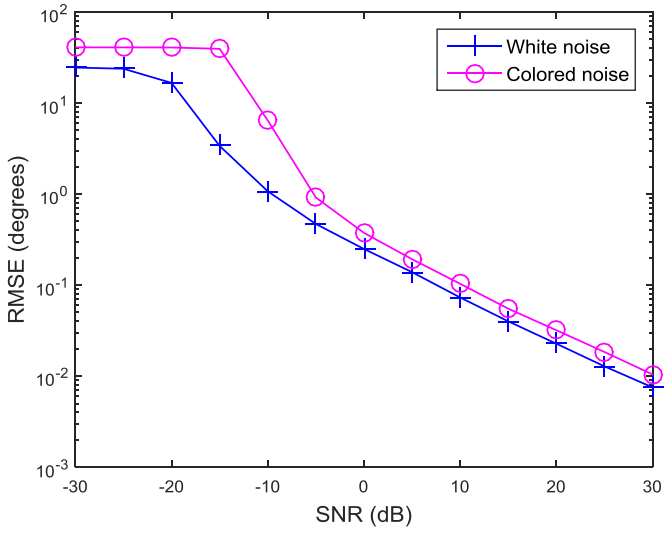

Fig. 11. DOA estimation performance of the proposed algorithm for white and colored noise.

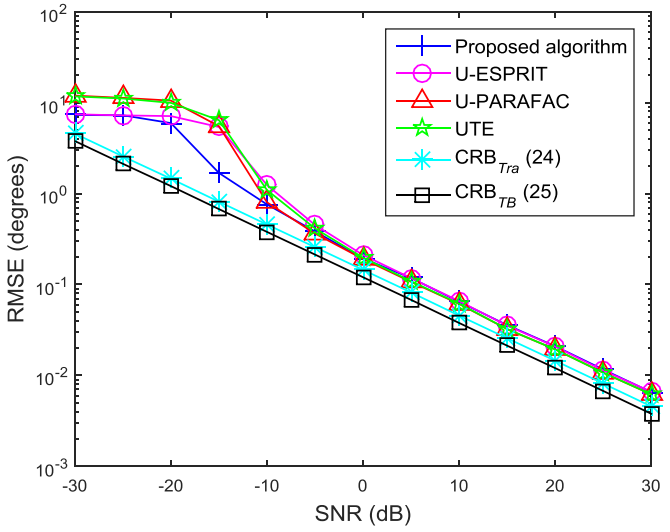

Fig. 12. RMSE of DOD versus SNR for two correlated targets (after the mapping operation).

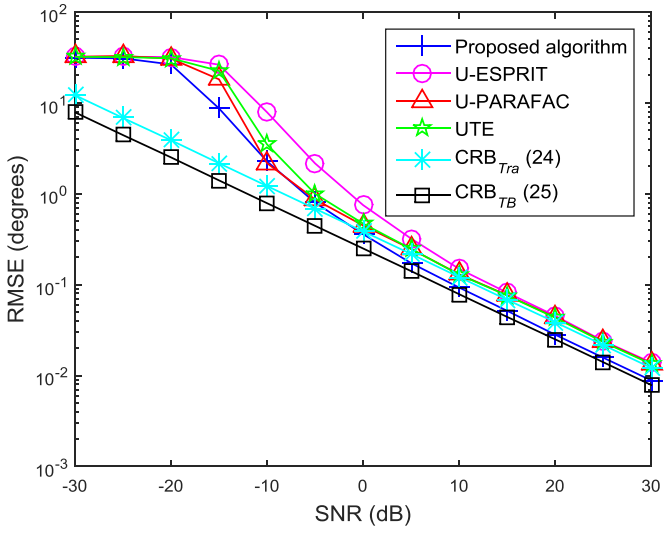

Fig. 13. RMSE of DOA versus SNR for two correlated targets.

called as SNR threshold. Compared with other methods, the proposed algorithm has the lowest SNR threshold. When SNR reaches 4 dB, the probability of successful detection of the proposed algorithm reaches 100%.

In the third example, the estimation performance of the proposed algorithm is assessed with spatial colored noise. In this case, the covariance matrix of $\overline{\mathbf{n}}_q$ in (5) can be written as $\mathbf{I}_L \otimes \mathbf{Q}$ according to [17], where $\mathbf{Q} \in \mathbb{C}^{N\times N}$ denotes a Hermitian symmetric Toeplitz matrix. The $(n_1, n_2)th$ element of $\mathbf{Q}$ is given by $\mathbf{Q}(n_1, n_2)=0.9^{|n_1-n_2|}e^{j\pi(n_1-n_2)/2}$. The other simulation conditions are similar with the second example. Figs. 10 and 11 respectively show the DOD and DOA estimation performance of the proposed algorithm for white and colored noise. We can find that when the additive noise is colored, the estimation performance of the proposed algorithm is degraded. This is because the signal subspace cannot be separated exactly from the noise subspace via the EVD method.

In the fourth example, we examine the estimation performance of the proposed algorithm for two correlated targets, which are located at $(\theta_1,\ \varphi_1) = (-10^\circ, -50^\circ)$ and $(\theta_2,\ \varphi_2) = (10^\circ, 10^\circ)$, respectively. The correlation coefficient between the two targets is fixed at 0.99. Fig. 12 shows the RMSE of DOD versus SNR after the mapping operation. Fig. 13 shows the RMSE of DOA versus SNR. The number of pulses is $Q = 50$. Exploiting the forward-backward averaging technique, all the tested methods have the decorrelation ability. However, the proposed algorithm still outperforms other methods especially at low SNR.

In the fifth example, there are two targets located at $(\theta_1,\ \varphi_1) = (-10^\circ, -40^\circ)$ and $(\theta_2,\ \varphi_2) = (10^\circ, 20^\circ)$, respectively. The correlation coefficient between the two targets is varied from 0 to 1. Fig. 14 shows the RMSE of DOD and DOA of all the methods. In this case, the number of pulses is $Q = 50$ and SNR is fixed at 10 dB. Although there exists performance degradation when the correlation coefficient approaches to 1, we can observe that the proposed algorithm still has better performance than other tested methods. Combining the TB technique with the U-ESPRIT model, the proposed algorithm can deal with two coherent targets with the improved SNR gain.

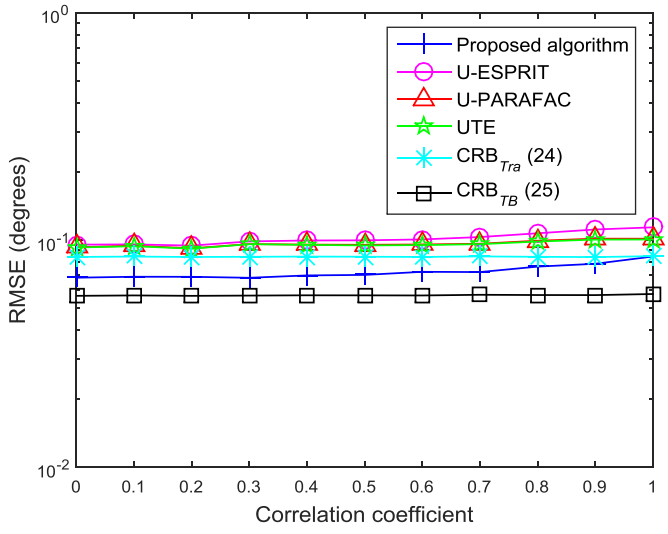

Fig. 14. RMSE versus the correlation coefficient between the two targets.

5. Conclusion

In this paper, a novel DOD and DOA estimation method is proposed for TB-based bistatic MIMO radar with white Gaussian noise. For the special data structure of the TB-based bistatic MIMO radar, a new way is proposed to construct the real-valued model. Combining the TB technique with the U-ESPRIT model, the proposed algorithm achieves the transmit coherent gain and can deal with two coherent targets. We also build a DOD look-up table to compensate the DOD estimation error. Compared with the traditional U-ESPRIT algorithm, the proposed algorithm has better estimation performance and requires less computational complexity. The CRB on DOD and DOA estimation for TB-based bistatic MIMO radar is also derived for performance analysis. The performance analysis of the proposed algorithm in spatial colored noise is also given. Numerical simulations are given to show the superior performance of the proposed algorithm.

Acknowledgments

This research did not receive any specific grant from funding agencies in the public, commercial, or not-for-profit sectors.

Appendix A

In Appendix A, we prove that the real-valued matrix $\mathbf{Z}$ in (13) can be rewritten as (14) if the interpolation error is neglected.

Substituting (6) to (12), we have

$$\begin{aligned}\overline{\mathbf{Y}} &= [\mathbf{Y},\ \ (\mathbf{I}_L \otimes \mathbf{\Pi}_N)\mathbf{Y}^*\mathbf{\Pi}_Q] \\ &= \sqrt{\frac{E}{L}}\Big[\big((\mathbf{W}^H\mathbf{A}) \odot \mathbf{B}\big)\mathbf{C},\ \ (\mathbf{I}_L \otimes \mathbf{\Pi}_N)\big((\mathbf{W}^H\mathbf{A})^* \odot \mathbf{B}^*\big)\mathbf{C}^*\mathbf{\Pi}_Q\Big] + \widehat{\mathbf{N}} \\ &= \sqrt{\frac{E}{L}}\Big[\big((\mathbf{W}^H\mathbf{A}) \odot \mathbf{B}\big)\mathbf{C},\ \ \big((\mathbf{W}^H\mathbf{A})^* \odot \mathbf{\Pi}_N\mathbf{B}^*\big)\mathbf{C}^*\mathbf{\Pi}_Q\Big] + \widehat{\mathbf{N}} \qquad \text{(A.1)}\end{aligned}$$

where $\widehat{\mathbf{N}} = [\widetilde{\mathbf{N}},\ \ (\mathbf{I}_L \otimes \mathbf{\Pi}_N)\widetilde{\mathbf{N}}^*\mathbf{\Pi}_Q]$. In the derivation of (A.1), we use the property that $(\mathbf{A} \otimes \mathbf{B})(\mathbf{C} \odot \mathbf{D}) = \mathbf{AC} \odot \mathbf{BD}$. Because each column in $\mathbf{B}$ is conjugate centrosymmetric, the matrix $\mathbf{B}$ satisfies $\mathbf{\Pi}_N\mathbf{B}^* = \mathbf{B}$. Then, (A.1) can be rewritten as

$$\begin{aligned}\overline{\mathbf{Y}} &= \sqrt{\frac{E}{L}}\Big[\big((\mathbf{W}^H\mathbf{A}) \odot \mathbf{B}\big)\mathbf{C},\ \ \big((\mathbf{W}^H\mathbf{A})^* \odot \mathbf{B}\big)\mathbf{C}^*\mathbf{\Pi}_Q\Big] + \widehat{\mathbf{N}} \\ &= \sqrt{\frac{E}{L}}\Big[\big(\mathrm{Re}\{\mathbf{W}^H\mathbf{A}\} \odot \mathbf{B}\big)\mathbf{C},\ \ \big(\mathrm{Re}\{\mathbf{W}^H\mathbf{A}\} \odot \mathbf{B}\big)\mathbf{C}^*\mathbf{\Pi}_Q\Big] \qquad \text{(A.2)} \\ &\quad + j\sqrt{\frac{E}{L}}\Big[\big(\mathrm{Im}\{\mathbf{W}^H\mathbf{A}\} \odot \mathbf{B}\big)\mathbf{C},\ \ -\big(\mathrm{Im}\{\mathbf{W}^H\mathbf{A}\} \odot \mathbf{B}\big)\mathbf{C}^*\mathbf{\Pi}_Q\Big] + \widehat{\mathbf{N}}\end{aligned}$$

Substituting (A.2) into (13), we obtain

$$\begin{aligned}\mathbf{Z} &= \big(\mathbf{I}_L \otimes \mathbf{U}_N^H\big)\overline{\mathbf{Y}}\mathbf{U}_{2Q} \\ &= \sqrt{\frac{E}{L}}\Big[\big(\mathrm{Re}\{\mathbf{W}^H\mathbf{A}\} \odot \mathbf{U}_N^H\mathbf{B}\big)\mathbf{C},\ \ \big(\mathrm{Re}\{\mathbf{W}^H\mathbf{A}\} \odot \mathbf{U}_N^H\mathbf{B}\big)\mathbf{C}^*\mathbf{\Pi}_Q\Big]\mathbf{U}_{2Q} \\ &\quad + j\sqrt{\frac{E}{L}}\Big[\big(\mathrm{Im}\{\mathbf{W}^H\mathbf{A}\} \odot \mathbf{U}_N^H\mathbf{B}\big)\mathbf{C},\ \ -\big(\mathrm{Im}\{\mathbf{W}^H\mathbf{A}\} \odot \mathbf{U}_N^H\mathbf{B}\big)\mathbf{C}^*\mathbf{\Pi}_Q\Big] \\ &\quad \mathbf{U}_{2Q} + \widehat{\mathbf{N}} \\ &= \sqrt{\frac{E}{L}}\big(\mathrm{Re}\{\mathbf{W}^H\mathbf{A}\} \odot \mathbf{U}_N^H\mathbf{B}\big)[\mathbf{C},\ \mathbf{C}^*\mathbf{\Pi}_Q]\mathbf{U}_{2Q} + \hat{\mathbf{N}} + \mathbf{\Gamma} \qquad \text{(A.3)}\end{aligned}$$

where $\hat{\mathbf{N}} = (\mathbf{I}_L \otimes \mathbf{U}_N^H)\widehat{\mathbf{N}}\mathbf{U}_{2Q}$ denotes the real-valued noise term and

$$\mathbf{\Gamma} = j\sqrt{\frac{E}{L}}\ \big(\mathrm{Im}\{\mathbf{W}^H\mathbf{A}\} \odot \mathbf{U}_N^H\mathbf{B}\big)[\mathbf{C},\ -\mathbf{C}^*\mathbf{\Pi}_Q]\mathbf{U}_{2Q} \qquad \text{(A.4)}$$

In (A.3), both $\mathbf{U}_N^H\mathbf{B}$ and $[\mathbf{C}, \mathbf{C}^*\mathbf{\Pi}_Q]\mathbf{U}_{2Q}$ are real-valued matrices because all columns of $\mathbf{B}$ and rows of $[\mathbf{C}, \mathbf{C}^*\mathbf{\Pi}_Q]$ are conjugate centrosymmetric. In (A.4), $[\mathbf{C}, -\mathbf{C}^*\mathbf{\Pi}_Q]\mathbf{U}_{2Q}$ is a complex matrix, whose real part is equal to zero. Consequently, $j[\mathbf{C}, -\mathbf{C}^*\mathbf{\Pi}_Q]\mathbf{U}_{2Q}$ is a real-valued matrix. This means that the matrix $\mathbf{\Gamma}$ is also a real-valued matrix.

From (A.3), we can also find that if the interpolation error is neglected, which means $\mathrm{Re}\{\mathbf{W}^H\mathbf{A}\} = \mathbf{U}_L^H\overline{\mathbf{A}}$ and $\mathrm{Im}\{\mathbf{W}^H\mathbf{A}\} = \mathbf{0}$, the real-valued matrix $\mathbf{\Gamma}$ is equal to zero. Here, $\overline{\mathbf{A}} = [\overline{\mathbf{a}}(\theta_1), \overline{\mathbf{a}}(\theta_2), \ldots, \overline{\mathbf{a}}(\theta_K)]$ denotes the virtual transmit steering matrix. Then, (A.3) can be reformulated as

$$\mathbf{Z} = \sqrt{\frac{E}{L}}\big(\mathrm{Re}\{\mathbf{W}^H\mathbf{A}\} \odot \mathbf{U}_N^H\mathbf{B}\big)[\mathbf{C}, \mathbf{C}^*\mathbf{\Pi}_Q]\mathbf{U}_{2Q} + \hat{\mathbf{N}} \qquad \text{(A.5)}$$

In (A.5), matrices $\mathrm{Re}\{\mathbf{W}^H\mathbf{A}\}$ and $\mathbf{U}_N^H\mathbf{B}$ respectively include DOD and DOA information, which can be extracted from $\mathbf{Z}$.

Appendix B

In Appendix B, we prove that the dominated eigenvector of $\mathbf{R}_{map}$ spans the same subspace with $\mathrm{Re}\{\mathbf{W}^H\mathbf{a}(\theta_i)\}$ in the desired spatial sector.

Similar with Appendix A, (21) can be rewritten as

$$\begin{aligned}\mathbf{Y}_{map} &= \big[\mathbf{W}^H\mathbf{a}(\theta_i)\mathbf{c},\ \ \big(\mathbf{W}^H\mathbf{a}(\theta_i)\mathbf{c}\big)^*\mathbf{\Pi}_Q\big]\mathbf{U}_{2Q} \\ &= \big[\mathrm{Re}\{\mathbf{W}^H\mathbf{a}(\theta_i)\}\mathbf{c},\ \mathrm{Re}\{\mathbf{W}^H\mathbf{a}(\theta_i)\}\mathbf{c}^*\mathbf{\Pi}_Q\big]\mathbf{U}_{2Q} \\ &\quad + j\big[\mathrm{Im}\{\mathbf{W}^H\mathbf{a}(\theta_i)\}\mathbf{c},\ -\mathrm{Im}\{\mathbf{W}^H\mathbf{a}(\theta_i)\}\mathbf{c}^*\mathbf{\Pi}_Q\big]\mathbf{U}_{2Q} \\ &= \mathrm{Re}\{\mathbf{W}^H\mathbf{a}(\theta_i)\}[\mathbf{c},\ \mathbf{c}^*\mathbf{\Pi}_Q]\mathbf{U}_{2Q} + \mathbf{\Xi} \qquad \text{(B.1)}\end{aligned}$$

where $\mathbf{c}$ denotes a $1 \times Q$ vector and $\mathbf{\Xi} = j\mathrm{Im}\{\mathbf{W}^H\mathbf{a}(\theta_i)\}[\mathbf{c}, -\mathbf{c}^*\mathbf{\Pi}_Q]\mathbf{U}_{2Q}$ is a real-valued matrix. $\mathbf{U}_{2Q}$ is a unitary matrix and there exists $\mathbf{U}_{2Q}\mathbf{U}_{2Q}^H = \mathbf{I}_{2Q}$. Hence, using (B.1), we have

$$\mathbf{R}_{map} = \frac{\delta}{2Q}\mathrm{Re}\{\mathbf{W}^H\mathbf{a}(\theta_i)\}\mathrm{Re}\{\mathbf{W}^H\mathbf{a}(\theta_i)\}^H + \frac{1}{2Q}\mathbf{\Xi}\,\mathbf{\Xi}^H \qquad \text{(B.2)}$$

where $\delta = \mathbf{c}\mathbf{c}^H + \mathbf{c}^*\mathbf{c}^T = 2\mathrm{Re}\{\mathbf{c}\mathbf{c}^H\}$ denotes a real-valued scalar. In the desired spatial sector, $\mathrm{Re}\{\mathbf{W}^H\mathbf{a}(\theta_i)\}$ is much larger than $\mathrm{Im}\{\mathbf{W}^H\mathbf{a}(\theta_i)\}$ because of the constraints in (10). Consequently, the dominated eigenvector of $\mathbf{R}_{map}$ spans the same subspace with $\mathrm{Re}\{\mathbf{W}^H\mathbf{a}(\theta_i)\}$ in the desired spatial sector.

References

[1] L. Xu, J. Li, P. Stoica, Target detection and parameter estimation for MIMO radar system, IEEE Trans. Aerosp. Electron. Syst. 44 (3) (2008) 927–939.
[2] I. Bekkerman, J. Tabrikian, Target detection and localization using MIMO radars and sonars, IEEE Trans. Signal Process. 54 (10) (2006) 3873–3883.
[3] E. Fisher, A. Haimovich, R. Blum, Spatial diversity in radars-models and detection performance, IEEE Trans. Signal Process. 54 (3) (2006) 823–838.
[4] E. Fishler, A. Haimovich, R. Blum, D. Chizhik, L. Cimini, R. Valenzuela, MIMO radar: an idea whose time has come, in: Proceedings of IEEE Radar Conference, 2004, pp. 71–78.
[5] A.M. Haimovich, R. Blum, L. Cimini, MIMO radar with widely separated antennas, IEEE Signal Process. Mag. 25 (1) (2008) 116–129.
[6] J. Li, P. Stoica, MIMO radar with colocated antennas, IEEE Signal Process. Mag. 24 (5) (2007) 106–114.
[7] H. Yan, J. Li, G. Liao, Multitarget identification and localization using bistatic MIMO radar systems, EURASIP J. Adv. Signal Process (2008) 1–8.
[8] M.L. Bencheikh, Y. Wang, H. He, Polynomial root finding technique for joint DOA DOD estimation in bistatic MIMO radar, Signal Process. 90 (2010) 2723–2730.
[9] C. Duofang, C. Baixiao, Q. Guodong, Angle estimation using ESPRIT in MIMO radar, Electron. Lett. 44 (12) (2008) 770–771.
[10] J. Chen, H. Gu, W. Su, Angle estimation using ESPRIT without pairing in MIMO radar, Electron. Lett. 44 (24) (2008) 1422–1423.
[11] G. Zheng, B. Chen, M. Yang, Unitary ESPRIT algorithm for bistatic MIMO radar, Electron. Lett. 48 (3) (2012) 179–181.
[12] Y. Cheng, R. Yu, H. Gu, W. Su, Multi-SVD based subspace estimation to improve angle estimation accuracy in bistatic MIMO radar, Signal Process 93 (7) (2013) 2003–2009.
[13] M. Haardt, F. Roemer, G.D. Galdo, Higher-order SVD-based subspace estimation to improve the parameter estimation accuracy in multidimensional harmonic retrieval problems, IEEE Trans. Signal Process. 56 (7) (2008) 3198–3213.
[14] D. Nion, N.D. Sidiropoulos, A PARAFAC-based technique for detection and localization of multiple targets in a MIMO radar system, in: in Proc. IEEE Int. Conf. Acoust., Speech, Signal Process, Taipei, Taiwan, 2009, pp. 2077–2080. April.
[15] B. Xu, Y. Zhao, Z. Cheng, H. Li, A novel unitary PARAFAC method for DOD and DOA estimation in bistatic MIMO radar, Signal Process. 138 (2017) 273–279.
[16] T.G. Kolda, B.W. Bader, Tensor decomposition and application, SIAM Rev. 51 (3) (2009) 455–500.
[17] F. Wen, X. Xiong, J. Su, Z. Zhang, Angle estimation for bistatic MIMO radar in the presence of spatial colored noise, Signal Process. 134 (2017) 261–267.
[18] A. Hassanien, S. Vorobyov, Transmit energy focusing for DOA estimation in MIMO radar with colocated antennas, IEEE Trans. Signal Process. 59 (6) (2011) 2669–2682.
[19] A. Khabbazibasmenj, A. Hassanien, S.A. Vorobyov, Efficient transmit beamspace design for search-free based DOA estimation in MIMO radar, IEEE Trans. Signal Process. 62 (6) (2014) 1490–1500.
[20] M.D. Zoltowski, M. Haardt, C.P. Mathews, Closed-form 2-D angle estimation with rectangular arrays in element space or beamspace via unitary ESPRIT, IEEE Trans. Signal Process. 44 (2) (1996) 316–328.
[21] L. Vandenberghe, S. Boyd, S.P. Wu, Determinant maximization with linear matrix inequality constraints, SIAM J. Matrix Anal. Appl. 19 (2) (1998) 499–533.
[22] M. Haardt, J.A. Nossek, Unitary ESPRIT: how to obtain increased estimation accuracy with a reduced computational burden, IEEE Trans, Signal Process. 43 (5) (1995) 1232–1242.
[23] M. Haardt, J.A. Nossek, Simultaneous Schur decomposition of several non-symmetric matrices to achieve automatic pairing in multidimensional harmonic retrieval problems, IEEE Trans. Signal Process. 46 (1) (1998) 161–169.
[24] X. Zhang, Z. Xu, L. Xu, D. Xu, Trilinear decomposition-based transmit angle and receive angle estimation for multiple-input multiple-output radar, IET Radar Sonar Navig. 5 (6) (2011) 626–631.
[25] P. Stoica, A. Nehorai, Performance study of conditional and unconditional direction-of-arrival estimation, IEEE Trans. Acoust. Speech Signal Process. 38 (10) (1990) 1783–1795.
[26] P. Hyberg, M. Jansson, B. Ottersten, Array interpolation and DOA MSE reduction, IEEE Trans. Signal Process. 53 (12) (2005) 4464–4471.